

# VP-LLM: Text-Driven 3D Volume Completion with Large Language Models through Patchification

Jianmeng Liu<sup>1\*</sup>, Yichen Liu<sup>1\*</sup>, Yuyao Zhang<sup>1\*</sup>, Zeyuan Meng<sup>1\*</sup>, Yu-Wing Tai<sup>2</sup>, Chi-Keung Tang<sup>1</sup>

<sup>1</sup>The Hong Kong University of Science and Technology  
<sup>2</sup>Dartmouth College

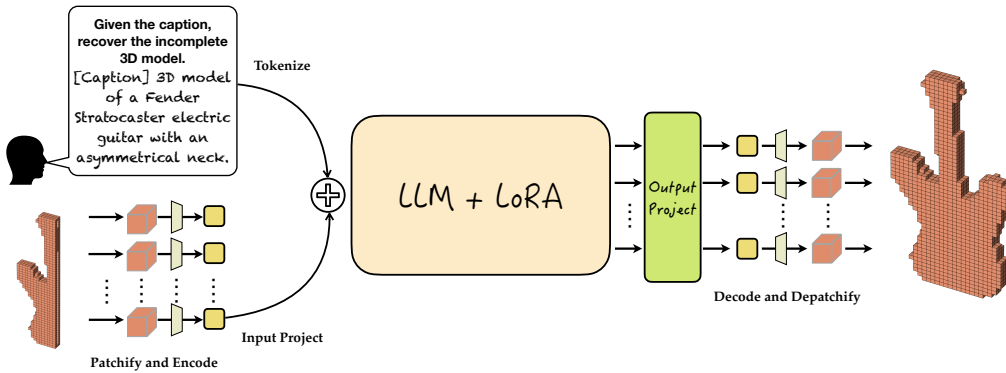


Figure 1: **Overview.** VP-LLM leverages the long-context comprehension capability of Large Language Models (LLMs) to process 3D models. It takes either incomplete or noisy 3D models along with textual instructions as input, and generate a complete model. This is achieved by segmenting the 3D object into patches and processing each independently.

## Abstract

Recent conditional 3D completion works have mainly relied on CLIP or BERT to encode textual information, which cannot support complex instruction. Meanwhile, large language models (LLMs) have shown great potential in multi-modal understanding and generation tasks. Inspired by the recent advancements of LLM, we present Volume Patch LLM (VP-LLM), which leverages LLMs to perform conditional 3D completion in a single-forward pass. To integrate a 3D model into the LLM tokenization configuration, the incomplete 3D object is first divided into small patches that can be encoded independently. These encoded patches are then fed into an LLM along with the text prompt, instructing the LLM to capture the relations between these patches as well as injecting semantic meanings into the 3D object. Our results demonstrate a strong ability of LLMs to interpret complex text instructions and understand 3D objects, surpassing state-of-the-art diffusion-based 3D completion models in generation quality.

\*Co-first authors, ranked by alphabetical order of first names

# 1 Introduction

3D modeling serves as a pivotal component in a multitude of 3D vision applications including robotics and virtual reality, where the quality of 3D data critically influences model performance. Despite the advancement in 3D scanning technology, the raw data acquired are often noisy, clustered, and may contain large portions of missing data due to occlusion, complex real-world scenes and restricted camera angles, resulting in incomplete 3D acquisition. This necessitates robust pre-processing to recover or complete the 3D objects, which can enhance the efficiency of subsequent 3D vision tasks.

Current approaches for 3D shape completion typically operate on a depth map or partial point cloud, converting it into a voxel representation or sampling points to restore the original 3D objects. While [58, 68] showcase advancements, they are confined to specific categories and lack the ability of cross-object generation. Although efforts have been made [61, 64, 57, 56] to create a unified model that handles multi-category 3D completion, these models often overlook the inclusion of textual input in guiding the completion process, leading to uncertainty when the input is ambiguous, as well as degradation of feasibility when given captions deviate from the training set. Consequently, methods are needed to generate a completed shape aligning precisely with the provided text description. Some attempts mimic the 2D diffusion method [10] or score distillation sampling (SDS) [24] to incorporate text guidance in the 3D completion tasks, but they cannot be precisely controlled when the description is complicated, and are very time-consuming to generate the results.

To this end, we propose Volume Patch Large Language Model (VP-LLM), which achieves 3D completion with precise textual control. Inspired by the recent progress in 3D multi-modality models [63, 9, 54], we believe that Large Language Models (LLMs) can underpin our approach by decoding the complex associations between 3D structures and textual descriptions. LLMs, pretrained on large-scale text datasets, have the capability to process long sequences and comprehend complex human languages, while 3D models represented by voxel grids can be straightforwardly converted into a one-dimensional format through flattening. Therefore, we investigate how to enable LLMs to understand a 3D model by decoding complex correlations between 3D structures and textual descriptions, or “translating” it into a “sentence”.

For seamless incorporation of 3D data into the LLM tokenization framework, 3D models are initially segmented into smaller patches, facilitating independent encoding and decoding. Different from most previous methods that manage the 3D object as a unified, this idea of patchification is more scalable and extendable. The patchified 3D voxel volume can be processed as a sequence and fed into the LLM with the textual description after alignment. The LLM can fuse the 3D and textural features into its hidden latents, which are finally decoded into complete 3D models.

Our whole pipeline is presented in Fig. 1. The 3D volumes are first patchified into individual patches and processed by a patch-wise Variational Autoencoder (VAE) to encode individually. The encoded patches are then projected and concatenated with user-specified text conditions to the LLM. Finally, the output projection layer extracts the features generated by the LLM and lets the VAE decode back each patch individually.

In summary, the major contributions of our papers are

1. VP-LLM is the first work leveraging *LLM* to achieve text-guided 3D completion, outperforming existing state-of-the-art text-conditioned 3D completion works.
2. The *patchification* method we proposed enables a scalable integration of 3D volumes into the LLM, solving the difficulty in handling high-resolution voxel grids faced by existing works.
3. Our work can perform 3D completion and denoising for multiple categories using detailed text control within one unified model.

Thus, this experimental paper offers insights and lessons learned, providing the first LLM solution to text-guided 3D object completion. Codes and data will be made public upon the paper’s acceptance.

## 2 Related Works

### 2.1 Multimodality Large Language Models

The advent of Large Language Models (LLMs) has significantly accelerated advancements in natural language processing. Several studies [22, 49, 48] have demonstrated the capabilities of LLM in comprehending long contexts, ensuring scalability and adaptability, and facilitating the understanding and generation of natural language. Benefiting from these advantages of LLM, many works have already employed LLM across different modalities, including images [53, 39, 1], motion [23], and video [67, 29]. Recently, several works combined LLM with 3D data. For example, [63] leverages a 3D-aware VQ-VAE [51] and integrates its codebook into the LLM’s vocabulary, enabling the LLM to generate and understand 3D objects. But the codebook size may bottleneck the capability of LLM to tackle 3D objects with more complex and various structures. LLM-Grounder [62] carefully designs LLM prompt to translate the instructions into regular sub-tasks and instructs some pre-trained 3D grounders [27, 40] for 3D reasoning, where 3D models are not integrated into the LLM. Octavius [9] adopts the object detector to first discover candidate regions, followed by the application of pre-trained point cloud encoders for extracting features at the instance level. These features are then aggregated and mapped into an LLM for diverse 3D understanding tasks. However, this process reduces the entire 3D model to a single feature, thereby omitting crucial detailed information. In contrast, VP-LLM employs a VAE [28] combined with projection layers, capable of effectively aligning the 3D latent space with the LLM’s text space, thus enhancing the model’s generalizability, especially for out-of-distribution data.

### 2.2 Text-to-3D Generation

Prior to the era of machine learning, primitive works attempted to retrieve 3D assets from large databases, such as [5, 4]. With the rise of GANs [16], attempts such as Text2Shape [7] started to dominate the 3D generation field. Recently, due to promising advancements in text-to-image generation, research focus on text-control 3D generation has shifted to diffusion model [18]. Some works [32, 44, 20] adopt CLIP [42] to align the rendered images with the input text, thus ensuring the semantic meaning of the 3D model, while others like [41, 55, 52, 8, 34, 3] leverage pre-trained 2D diffusion models to provide text control and score distillation sampling to improve the 3D consistency. Although text-to-3D generation serves as an inspiration for text-guided 3D completion, none of the existing methods employ large language models for 3D-text interaction to guide the completion results.

### 2.3 3D Completion

3D completion is a crucial process in various industries, enabling accurate and efficient design and production, and enhancing the overall quality of products and projects. Early works such as [11, 13, 15, 17, 45, 46, 60] that use 3D convolutions with structured representation require high memory usage and compute. Followed by [66], many works [2, 47, 65, 58] that adopt point clouds as 3D representation for shape completion were proposed. For example, [2, 47, 65] generate the final shape in an auto-regressive manner, while [58] uses GANs [16] to complete the model. But none of these offer satisfactory user control. With the introduction of DDPM [18], works such as [31, 33, 36, 50, 59, 69, 10, 30] have advanced the 3D shape completion pipelines. Notably, [10] adopts a 3D diffusion model with VAE to achieve 3D completion with multi-type control, and [25] uses score distillation to perform test-time optimization. However, neither of them can perform completion tasks at a larger scale where model details are required, nor even generate satisfactory results without tedious denoising steps. Thus, scalability, speed and level of control are still issues to be addressed, providing strong motivation for our work.

## 3 Methodology

Given an incomplete 3D model and user-supplied textual description of the target 3D model, our model aims to recover the underlying 3D model aligned with the input text. First, the incomplete 3D model undergoes *patchification*, where it is split into small patches, and each patch is independently encoded by our Variational Autoencoder (VAE). Next, a shared-weight linear layer maps the patch

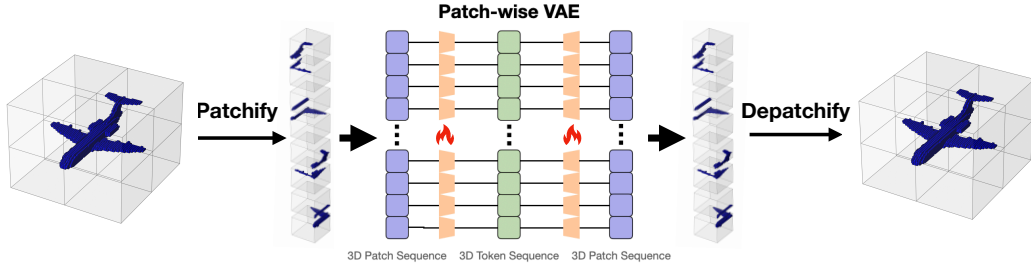


Figure 2: **Patchification**: given a 3D object, we first fit it into a voxel grid and then divide it into a sequence of small patches. Next, we utilize a patch-wise Variational Autoencoder (VAE) to extract the features of each patch individually and then reconstruct it back. It is important to note that only one VAE is trained for all the patches throughout the entire dataset, making our method a scalable approach.

features to the embedding space of the LLM, which are then combined with the textual description and input into the LLM. The LLM, concatenated with our specially-designed output projection layer, generates the features of patches at all positions, allowing for the separate decoding and subsequent assembly, or de-patchification, to the underlying complete 3D model.

### 3.1 Patchification

The first step of our method is to divide the 3D models into small patches, dubbed patchification. Figure 2 demonstrates the process of patchification. For a 3D object represented in voxel  $V \in \{0, 1\}^{H \times W \times D}$ ,  $V(x, y, z) = 1$  if the position  $x, y, z$  is occupied and 0 otherwise. Patchification uniformly partitions the 3D voxel volume into  $p$  small patches of the same size, each containing a local region of the entire object. For each patch  $P_{i,j,k} \in \{0, 1\}^{h \times w \times d}$ , the coordinate for position  $(x, y, z)$ ,  $0 \leq x \leq h, 0 \leq y \leq w, 0 \leq z \leq d$  is:

$$P_{i,j,k}(x, y, z) = V(i \cdot h + x, j \cdot w + y, k \cdot d + z). \quad (1)$$

Thus,  $p = \lfloor H/h \rfloor \cdot \lfloor W/w \rfloor \cdot \lfloor D/d \rfloor$ . In our experiments, we set  $H = W = D = 64$  and  $h = w = d = 8$ .

After patchification, a patch Variational Autoencoder (VAE) is adopted to extract the feature for each patch independently. Our patch VAE consists of an encoder  $\mathbf{E}$  and a decoder  $\mathbf{D}$ , where  $\mathbf{E}$  encodes a patch into a Gaussian distribution  $\mathcal{N}(\mu, \sigma)$  where  $\mu$  and  $\sigma$  are mean and variance, respectively, and  $\mathbf{D}$  recovers the original patch from this distribution. The VAE training loss for a single patch  $P$  is defined as

$$\mathcal{L}_{VAE}(P) = \mathcal{L}_{BCE}(P, \mathbf{D}(\mathbf{E}(P))) + \beta \mathcal{L}_{klD}(\mathbf{E}(P)), \quad (2)$$

where  $\mathcal{L}_{BCE}$  is the binary cross entropy loss,  $\mathcal{L}_{klD}$  is the KL-divergence and  $\beta$  is a hyperparameter.

Benefiting from this patchification structure that allows for independent encoding and decoding of each patch, VP-LLM ensures that when the completions of certain patches are undesired, they do not affect the performance of other well-performed patches, solving the problems faced by previous works that encode or decode the entire scene collectively.

### 3.2 Mask Strategy

To enhance the understanding of incomplete 3D models, we designed three different strategies to mask out different parts of the original 3D input, aiming to mimic the possible user inputs during the inference stage. Specifically, the following three strategies will be applied randomly with the same possibility:

1. *Random Mask*: Given the input 3D model in  $p$  patches, we randomly set  $m_r \cdot p$  patches to 0 (unoccupied), where  $m_r$  is a mask ratio sampled within a pre-defined range;

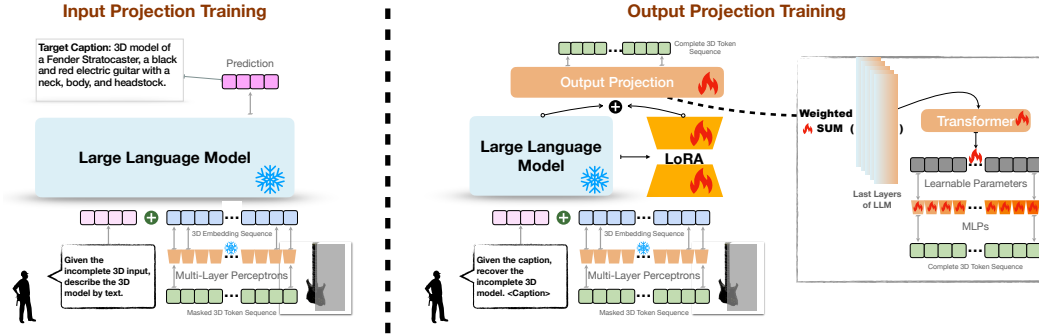


Figure 3: The training process of the **input projection** (left) and **output projection** (right). During the input projection training, a single share-weighted MLP maps the masked or noisy 3D tokens encoded by our patch-wise VAE to the embedding space of the LLM. After wrapping the prompt with the 3D tokens as input and feeding them to the LLM, we back-propagate the loss calculated between the ground-truth caption and the LLM’s prediction, enabling the LLM to learn to generate captions that accurately describe the 3D object from the input patches. For the output projection, we freeze the input projection layer and train the output projection layer, while also fine-tuning the LLM with LoRA. The output projection layer comprises a Transformer and a cluster of MLPs, such that after passing the Transformer, every 3D token is processed independently with an MLP.

2. *Plane Mask*: Given the input 3D model represented in voxel  $V(x, y, z)$ , we first project the model onto  $x$ -axis and find the first and last occupied voxels, denoted as  $x_1$  and  $x_2$ , along  $x$ -axis. Next, a plane parallel to  $yOz$  is sampled with  $x$ -coordinate between  $[x_1, x_2]$ . Intuitively, such a plane cuts the 3D model into two parts, and we then discard one of them by setting all voxels to be 0 (unoccupied) to simulate large portions of missing data in real capture;
3. *Random Noise*: Since real-world 3D models usually contain noises and artifacts, we mimic this situation by randomly inverting voxel occupancy (setting occupied voxels to be unoccupied, and vice versa). The noise level is also sampled in a pre-defined range indicating how many voxels to invert.

### 3.3 Input Projection Layer Training

The input project layer, which can map the VAE latent space into the LLM input embedding space, is a single linear model operated on each VAE latent patch. After patchifying and encoding the incomplete 3D model, each patch, represented by its respective  $\mu$  and  $\sigma$ , is first reparameterized into a single feature  $f$  by sampling from the Gaussian distribution  $\mathcal{N}(\mu, \sigma)$ . The feature (or each encoded patch) going through the input projection layer becomes a 3D token, which then can be understood by the LLM. To train the input projection layer, the LLM is instructed to predict the caption of the incomplete 3D model, given the prompt “Given the incomplete 3D input, describe the 3D model by text.” We use the training loss in [43] which is the negative log-likelihood on the caption. We use the training loss from the LLM to supervise this stage of training.

### 3.4 Output Projection Layer Training

The LLM, with the output projection layer appended, takes as input the tokenized sequence of the underlying incomplete 3D model, the user-supplied caption of the complete model as well as the instructions for completion, and outputs the complete 3D model aligned with the textual description. To be specific, we formulate the prompt for LLM as “Given the caption, recover the incomplete 3D model, <tokenized incomplete 3D sequence>, <Caption>”. The output projection layer architecture employs a transformer consisting of a 2-layer encoder and a 2-layer decoder, translating the LLM hidden states into a sequence of separable latent codes. We observe that to sufficiently explore the highly fused information in the LLM, more layers of hidden states are necessary. Thus, we select 5 layers in our experiments, which balances the amount of information with computational complexity. To ensure the length of the generated sequence, we set

Table 1: **Quantitative results compared with SDFusion and 3DQD.** We can observe that our method consistently hits the lowest (best) Chamfer Distance (CD) and the highest (best) CLIP-s score compared with SDFusion (text-conditioned completion) and 3DQD (label-conditioned completion). Moreover, our method is capable of denoising extremely noisy 3D inputs, while the baselines cannot accomplish the task.

Methods	Seg 20%		Seg 50%		Seg 80%		Noise 1%		Noise 2%	
	CD.↓	CLIP-s.↑	CD.↓	CLIP-s.↑	CD.↓	CLIP-s.↑	CD.↓	CLIP-s.↑	CD.↓	CLIP-s.↑
Ours	<b>10.96</b>	<b>27.80%</b>	<b>11.37</b>	<b>27.71%</b>	<b>17.42</b>	<b>25.17%</b>	16.03	23.92%	34.44	23.07%
SDFusion	95.44	26.66%	137.31	26.20%	235.98	22.22%	–	–	–	–
3DQD	172.89	22.63%	170.20	22.62%	196.12	22.62%	–	–	–	–

an additional learnable token sequence as the target. We then utilize Multi-layer Perceptrons (MLPs) to individually map each token to the desired 3D token. The final result is obtained through the concatenation of the mapped tokens.

During training, the input projection layer is frozen, while the LLM is finetuned with LoRA [19], while the output projection layer is trained from scratch. We use mean-squared error (MSE) loss between the output projection layer output and the VAE latent of ground-truth 3D model patches to update our model.

## 4 Experiments

### 4.1 Dataset

We train our model on a subset of ShapeNet [6] dataset, comprising over 3000 objects. To obtain the detailed textual description of 3D models in human languages, we adopt Cap3D [37], which leverages BLIP to predict and GPT-4 to refine captions for 3D models. In our experiments, the resolutions of the 3D voxels and patches are respectively set as  $64 \times 64 \times 64$  and  $8 \times 8 \times 8$ , while we explore the capability of the model to handle higher resolution formats in Sec. 5.2.

To improve the robustness of our model, we apply data augmentation during training. For the 3D models, we rotate them along one random axis with an arbitrary angle making the order of sequence different, while for the captions of the 3D model, we adjust the GPT configurations in Cap3D. Only 3D data augmentation is used in input projection training, while both 3D data and caption augmentation are used in output projection training. More details of the data augmentation can be found in Appendix C.

### 4.2 Comparison

We compare our model with SDFusion [10] and 3DQD [30], which are two state-of-the-art diffusion-based methods on conditional 3D completion tasks. SDFusion accepts multi-modality input for shape completion, so in our case, we only enable text-conditioned completion and enforce no image condition.

The quantitative comparison results are shown in Tab. 1. Following [12, 30], we use Chamfer Distance (CD) and CLIP-s score for evaluation. For Chamfer Distance, we transform our volume representation into point clouds and use the coordinates in the voxel grids. For the CLIP-s score, we render 20 different-view 2D images around each volume and take the maximums among the CLIP feature scores between the images and the textual description. We test the performance of the models under various circumstances, by segmenting the different fractions of the object and adding random noise to the objects. We also provide visualization results in Tab. 2 and Tab. 3.

It is worth noticing that 3DQD is a label-conditional completion model that does not include detailed text control during inference, leading to large variance in the prediction results. Though SDFusion contains text control in completion, it adopts BERT [14] for text encoding, thereby suffering from complex text understanding.

More qualitative results are presented in Appendix E.

Table 2: **Comparison of our method with SDFusion and 3DQD, on Airplane dataset.** We can clearly see our method outperforms their methods when the input is segmented by a plane and performs reasonably well when the input is added with noises. Since the two baselines cannot work on noisy inputs, “N/A” is placed instead.

	Ground Truth	Masked/Noisy	Ours	SDFusion	3DQD
Seg 20%					
	<i>“3D model of a Boeing 747-400 featuring a spherical fuselage shell, truncated oblate wings, and made of aluminum and steel.”</i>				
Seg 50%					
	<i>“3D model of a toy airplane featuring a wing, fuselage, tail, rudder, and propeller, available in 3ds Max, OBJ, FBX, and C4D formats.”</i>				
Seg 80%					
	<i>“Royalty-free 3D model of a stealth fighter jet, featuring a delta wing with horizontal and vertical stabilizers”</i>				
Noise 1%				N/A	N/A
	<i>“3D model of a Saber fighter jet featuring detailed wings, fuselage, and multiple landing gears, compatible with 3ds Max, Maya, Blender, and other 3D software.”</i>				
Noise 2%				N/A	N/A
	<i>“Royalty-free 3D model of a Boeing 747-400 jumbo jet.”</i>				

## 5 Ablation Study

### 5.1 Comparison of different LLM architectures

LLM is one of the most important components in our model, whose ability to capture multi-modal semantic information and token relations may greatly affect the performance of the entire pipeline. To investigate the effect of different LLMs on the performance of our model, we re-trained our method on Mistral-7B [21] and Gemma-2B [48]. To ensure a fair comparison, we keep the LoRA ranks for the two models to be the same. From Tab. 5.1, we find that under this setting, the two LLMs demonstrate similar results on mask completion, while the performance of Gemma-2B is better than Mistral-7B on denoising tasks while slightly worse in completion from masked inputs. Higher performance can be expected if larger LLM models or higher LoRA ranks are deployed.

### 5.2 Scalability on Higher Resolution Voxel Volumes

Our VAE encodes and decodes each patch of the 3D model individually, thus enabling our model to scale to higher voxel resolutions. To demonstrate the scalability, we have expanded upon our previous experiments by setting  $H = W = D = 64$ , and further increasing the voxel resolution to  $H = W = D = 72$ , while maintaining the patch size at 8. By fixing the patch size, we can ensure that the fine details of the data remain consistent as we increase the input scale. After this operation, the sequence length of each 3D object will increase from 512 to 729. We can see from Tab. 5 that the

Table 3: **Comparison of our method with SDFusion and 3DQD, on Car dataset.** We can clearly see our method outperforms their methods when the input is segmented by a plane and performs reasonably well when the input is added with noises. Since the two baselines cannot work on noisy inputs, “N/A” is placed instead.

	Ground Truth	Masked/Noisy	Ours	SDFusion	3DQD
Seg 20%					
	<i>“3D model of a Chevrolet Tahoe pickup truck in black and red, available in multiple formats including OBJ and FBX.”</i>				
Seg 50%					
	<i>“Royalty-free 3D model of a Mercedes-Benz SLK sports car”</i>				
Seg 80%					
	<i>“3D model of a muscle car with a hood, fenders, and a hood scoop.”</i>				
Noise 1%				N/A	N/A
	<i>“3D model of a yellow Dodge Viper SRT10 sports car.”</i>				
Noise 2%				N/A	N/A
	<i>“A 3D model of a police car, available royalty-free, with previews from different angles.”</i>				

Table 4: **Comparison using different LLM structures.** We utilize two LLMs, namely Mistral-7B and Gemma-2B, to train our whole pipeline with the same dataset as before. For comparison purposes, we demonstrate the Chamfer Distance (CD) and CLIP-s score on data containing 1% noise and 20% mask.

Methods	Seg 20%		Noise 1%	
	CD.↓	CLIP-s.↑	CD.↓	CLIP-s.↑
Mistral-7B	<b>10.96</b>	27.80%	16.03	23.92%
Gemma-2B	11.19	<b>28.08%</b>	<b>10.64</b>	<b>26.34%</b>

Table 5: **Comparison on different voxel volume resolutions.** We selected two different voxel volume resolutions, namely  $H = W = D = 64$  and  $H = W = D = 72$ . We can see the two resolutions have comparable results. Thanks to our patchification method that enables each patch to be processed and generated independently, our method perfectly scales when the resolution is larger.

Methods	Seg 20%		Noise 1%	
	CD.↓	CLIP-s.↑	CD.↓	CLIP-s.↑
Resolution 64 <sup>3</sup>	10.96	27.80%	16.03	23.92%
Resolution 72 <sup>3</sup>	12.33	27.38%	12.11	27.05%

two resolutions have comparable results, indicating our method can successfully generalize to higher voxel volume resolutions.

## 6 Limitation

Our method has been proven effective on small LLMs such as Mistral-7B. However, due to the limitation of computational resources, LLMs with stronger capability to understand long sequences, such as 70B or larger scale models, are not employed in our model. Thus, huge potential of our method is still left to probe. Additionally, though we verify the effectiveness of our method by patchification on voxel volumes, which can be intuitively extended to point clouds and SDFs, it is still very hard to employ it on those nascent 3D representations like NeRF [38] and 3D Gaussian Splatting (3DGS [26]) that encoded 3D in an implicit (MLP weights for NeRF and Gaussians for 3DGS). More investigations on how to patchify such representations are left in future works.

## 7 Conclusion

In this paper, we present VP-LLM, which combines text and 3D through LLMs to achieve text-guided 3D completion. We introduce a novel approach called patchification to incorporate 3D models into LLMs, and adopt a two-stage training process that allows LLMs to understand input incomplete 3D models and generate entire 3D models. Such an approach also allows an independent encoding and decoding process, thereby ensuring the scalability of our method. Experiments on the ShapeNet dataset validate that our method surpasses the state-of-the-art methods in the 3D completion task. Moreover, our model can achieve satisfactory results from noisy 3D inputs, a practical issue in real 3D data capture.

## References

- [1] Jean-Baptiste Alayrac, Jeff Donahue, Pauline Luc, Antoine Miech, Iain Barr, Yana Hasson, Karel Lenc, Arthur Mensch, Katie Millican, Malcolm Reynolds, Roman Ring, Eliza Rutherford, Serkan Cabi, Tengda Han, Zhitao Gong, Sina Samangooei, Marianne Monteiro, Jacob Menick, Sebastian Borgeaud, Andrew Brock, Aida Nematzadeh, Sahand Sharifzadeh, Mikolaj Binkowski, Ricardo Barreira, Oriol Vinyals, Andrew Zisserman, and Karen Simonyan. Flamingo: a visual language model for few-shot learning. *arXiv preprint arXiv:2204.14198*, 2022.
- [2] Li An, Pengbo Zhou, Mingquan Zhou, Yong Wang, and Qi Zhang. Pointtr: Low-overlap point cloud registration with transformer. *IEEE Sensors Journal*, 2024.
- [3] Sudarshan Babu, Richard Liu, Avery Zhou, Michael Maire, Greg Shakhnarovich, and Rana Hanocka. Hyperfields: Towards zero-shot generation of nerfs from text. *arXiv preprint arXiv:2310.17075*, 2023.
- [4] Angel Chang, Will Monroe, Manolis Savva, Christopher Potts, and Christopher D Manning. Text to 3d scene generation with rich lexical grounding. *arXiv preprint arXiv:1505.06289*, 2015.
- [5] Angel Chang, Manolis Savva, and Christopher D Manning. Learning spatial knowledge for text to 3d scene generation. In *Proceedings of the 2014 Conference on Empirical Methods in Natural Language Processing (EMNLP)*, pages 2028–2038, 2014.
- [6] Angel X Chang, Thomas Funkhouser, Leonidas Guibas, Pat Hanrahan, Qixing Huang, Zimo Li, Silvio Savarese, Manolis Savva, Shuran Song, Hao Su, et al. Shapenet: An information-rich 3d model repository. *arXiv preprint arXiv:1512.03012*, 2015.
- [7] Kevin Chen, Christopher B Choy, Manolis Savva, Angel X Chang, Thomas Funkhouser, and Silvio Savarese. Text2shape: Generating shapes from natural language by learning joint embeddings. In *Computer Vision—ACCV 2018: 14th Asian Conference on Computer Vision, Perth, Australia, December 2–6, 2018, Revised Selected Papers, Part III 14*, pages 100–116. Springer, 2019.
- [8] Rui Chen, Yongwei Chen, Ningxin Jiao, and Kui Jia. Fantasia3d: Disentangling geometry and appearance for high-quality text-to-3d content creation. In *Proceedings of the IEEE/CVF International Conference on Computer Vision*, pages 22246–22256, 2023.
- [9] Zeren Chen, Ziqin Wang, Zhen Wang, Huayang Liu, Zhenfei Yin, Si Liu, Lu Sheng, Wanli Ouyang, Yu Qiao, and Jing Shao. Octavius: Mitigating task interference in mllms via moe. *arXiv preprint arXiv:2311.02684*, 2023.
- [10] Yen-Chi Cheng, Hsin-Ying Lee, Sergey Tulyakov, Alexander G Schwing, and Liang-Yan Gui. Sdfusion: Multimodal 3d shape completion, reconstruction, and generation. In *Proceedings of the IEEE/CVF Conference on Computer Vision and Pattern Recognition*, pages 4456–4465, 2023.

- [11] Christopher B Choy, Danfei Xu, JunYoung Gwak, Kevin Chen, and Silvio Savarese. 3d-r2n2: A unified approach for single and multi-view 3d object reconstruction. In *Computer Vision—ECCV 2016: 14th European Conference, Amsterdam, The Netherlands, October 11-14, 2016, Proceedings, Part VIII 14*, pages 628–644. Springer, 2016.
- [12] Ruikai Cui, Weizhe Liu, Weixuan Sun, Senbo Wang, Taizhang Shang, Yang Li, Xibin Song, Han Yan, Zhennan Wu, Shenzhou Chen, et al. Neusdfusion: A spatial-aware generative model for 3d shape completion, reconstruction, and generation. *arXiv preprint arXiv:2403.18241*, 2024.
- [13] Angela Dai, Charles Ruizhongtai Qi, and Matthias Nießner. Shape completion using 3d-encoder-predictor cnns and shape synthesis. In *Proceedings of the IEEE conference on computer vision and pattern recognition*, pages 5868–5877, 2017.
- [14] Jacob Devlin, Ming-Wei Chang, Kenton Lee, and Kristina Toutanova. Bert: Pre-training of deep bidirectional transformers for language understanding. *arXiv preprint arXiv:1810.04805*, 2018.
- [15] Rohit Girdhar, David F Fouhey, Mikel Rodriguez, and Abhinav Gupta. Learning a predictable and generative vector representation for objects. In *Computer Vision—ECCV 2016: 14th European Conference, Amsterdam, The Netherlands, October 11-14, 2016, Proceedings, Part VI 14*, pages 484–499. Springer, 2016.
- [16] Ian Goodfellow, Jean Pouget-Abadie, Mehdi Mirza, Bing Xu, David Warde-Farley, Sherjil Ozair, Aaron Courville, and Yoshua Bengio. Generative adversarial nets. In *Advances in neural information processing systems*, volume 27, 2014.
- [17] Xiaoguang Han, Zhen Li, Haibin Huang, Evangelos Kalogerakis, and Yizhou Yu. High-resolution shape completion using deep neural networks for global structure and local geometry inference. In *Proceedings of the IEEE international conference on computer vision*, pages 85–93, 2017.
- [18] Jonathan Ho, Ajay Jain, and Pieter Abbeel. Denoising diffusion probabilistic models. *Advances in neural information processing systems*, 33:6840–6851, 2020.
- [19] Edward J Hu, Yelong Shen, Phillip Wallis, Zeyuan Allen-Zhu, Yuanzhi Li, Shean Wang, Lu Wang, and Weizhu Chen. Lora: Low-rank adaptation of large language models. *arXiv preprint arXiv:2106.09685*, 2021.
- [20] Ajay Jain, Ben Mildenhall, Jonathan T Barron, Pieter Abbeel, and Ben Poole. Zero-shot text-guided object generation with dream fields. In *Proceedings of the IEEE/CVF conference on computer vision and pattern recognition*, pages 867–876, 2022.
- [21] Albert Q Jiang, Alexandre Sablayrolles, Arthur Mensch, Chris Bamford, Devendra Singh Chaplot, Diego de las Casas, Florian Bressand, Gianna Lengyel, Guillaume Lample, Lucile Saulnier, et al. Mistral 7b. *arXiv preprint arXiv:2310.06825*, 2023.
- [22] Albert Q. Jiang, Alexandre Sablayrolles, Arthur Mensch, Chris Bamford, Devendra Singh Chaplot, Diego de las Casas, Florian Bressand, Gianna Lengyel, Guillaume Lample, Lucile Saulnier, Léo Renard Lavaud, Marie-Anne Lachaux, Pierre Stock, Teven Le Scao, Thibaut Lavril, Thomas Wang, Timothée Lacroix, and William El Sayed. Mistral 7b. *arXiv preprint arXiv:2310.06825*, 2023.
- [23] Biao Jiang, Xin Chen, Wen Liu, Jingyi Yu, Gang Yu, and Tao Chen. Motiongpt: Human motion as a foreign language. *arXiv preprint arXiv:2306.14795*, 2023.
- [24] Yoni Kasten, Ohad Rahamim, and Gal Chechik. Point cloud completion with pretrained text-to-image diffusion models. In A. Oh, T. Naumann, A. Globerson, K. Saenko, M. Hardt, and S. Levine, editors, *Advances in Neural Information Processing Systems*, volume 36, pages 12171–12191. Curran Associates, Inc., 2023.
- [25] Yoni Kasten, Ohad Rahamim, and Gal Chechik. Point cloud completion with pretrained text-to-image diffusion models. *Advances in Neural Information Processing Systems*, 36, 2024.
- [26] Bernhard Kerbl, Georgios Kopanas, Thomas Leimkühler, and George Drettakis. 3d gaussian splatting for real-time radiance field rendering. *ACM Transactions on Graphics*, 42(4), July 2023.
- [27] Justin Kerr, Chung Min Kim, Ken Goldberg, Angjoo Kanazawa, and Matthew Tancik. Lorf: Language embedded radiance fields. In *Proceedings of the IEEE/CVF International Conference on Computer Vision*, pages 19729–19739, 2023.
- [28] Diederik P Kingma and Max Welling. Auto-encoding variational bayes. *arXiv preprint arXiv:1312.6114*, 2013.
- [29] KunChang Li, Yanan He, Yi Wang, Yizhuo Li, Wenhai Wang, Ping Luo, Yali Wang, Limin Wang, and Yu Qiao. Videochat: Chat-centric video understanding. *arXiv preprint arXiv:2305.06355*, 2024.
- [30] Yuhan Li, Yishun Dou, Xuanhong Chen, Bingbing Ni, Yilin Sun, Yutian Liu, and Fuzhen Wang. 3dqd: Generalized deep 3d shape prior via part-discretized diffusion process. *arXiv preprint arXiv:2303.10406*, 2023.

- [31] Yuhan Li, Yishun Dou, Xuanhong Chen, Bingbing Ni, Yilin Sun, Yutian Liu, and Fuzhen Wang. Generalized deep 3d shape prior via part-discretized diffusion process. In *Proceedings of the IEEE/CVF Conference on Computer Vision and Pattern Recognition*, pages 16784–16794, 2023.
- [32] Jianmeng Liu, Yuyao Zhang, Zeyuan Meng, Yu-Wing Tai, and Chi-Keung Tang. Prompt2nerf-pil: Fast nerf generation via pretrained implicit latent. *arXiv preprint arXiv:2312.02568*, 2023.
- [33] Zhen Liu, Yao Feng, Michael J Black, Derek Nowrouzezahrai, Liam Paull, and Weiyang Liu. Meshdiffusion: Score-based generative 3d mesh modeling. *arXiv preprint arXiv:2303.08133*, 2023.
- [34] Jonathan Lorraine, Kevin Xie, Xiaohui Zeng, Chen-Hsuan Lin, Towaki Takikawa, Nicholas Sharp, Tsung-Yi Lin, Ming-Yu Liu, Sanja Fidler, and James Lucas. Att3d: Amortized text-to-3d object synthesis. In *Proceedings of the IEEE/CVF International Conference on Computer Vision*, pages 17946–17956, 2023.
- [35] Ilya Loshchilov and Frank Hutter. Decoupled weight decay regularization. *arXiv preprint arXiv:1711.05101*, 2017.
- [36] Shitong Luo and Wei Hu. Diffusion probabilistic models for 3d point cloud generation. In *Proceedings of the IEEE/CVF Conference on Computer Vision and Pattern Recognition*, pages 2837–2845, 2021.
- [37] Tiange Luo, Chris Rockwell, Honglak Lee, and Justin Johnson. Scalable 3d captioning with pretrained models. *Advances in Neural Information Processing Systems*, 36, 2024.
- [38] Ben Mildenhall, Pratul P. Srinivasan, Matthew Tancik, Jonathan T. Barron, Ravi Ramamoorthi, and Ren Ng. Nerf: Representing scenes as neural radiance fields for view synthesis. In *ECCV*, 2020.
- [39] OpenAI, Josh Achiam, Steven Adler, Sandhini Agarwal, Lama Ahmad, Ilge Akkaya, Florencia Leoni Aleman, Diogo Almeida, Janko Altmenschmidt, Sam Altman, Shyamal Anadkat, Red Avila, Igor Babuschkin, Suchir Balaji, Valerie Balcom, Paul Baltescu, Haiming Bao, Mohammad Bavarian, Jeff Belgum, Irwan Bello, Jake Berdine, Gabriel Bernadett-Shapiro, Christopher Berner, Lenny Bogdonoff, Oleg Boiko, Madelaine Boyd, Anna-Luisa Brakman, Greg Brockman, Tim Brooks, Miles Brundage, Kevin Button, Trevor Cai, Rosie Campbell, Andrew Cann, Brittany Carey, Chelsea Carlson, Rory Carmichael, Brooke Chan, Che Chang, Fotis Chantzis, Derek Chen, Sully Chen, Ruby Chen, Jason Chen, Mark Chen, Ben Chess, Chester Cho, Casey Chu, Hyung Won Chung, Dave Cummings, Jeremiah Currier, Yunxing Dai, Cory Decareaux, Thomas Degry, Noah Deutsch, Damien Deville, Arka Dhar, David Dohan, Steve Dowling, Sheila Dunning, Adrien Ecoffet, Atty Eleti, Tyna Eloundou, David Farhi, Liam Fedus, Niko Felix, Simón Posada Fishman, Juston Forte, Isabella Fullford, Leo Gao, Elie Georges, Christian Gibson, Vik Goel, Tarun Gogineni, Gabriel Goh, Rapha Gontijo-Lopes, Jonathan Gordon, Morgan Grafstein, Scott Gray, Ryan Greene, Joshua Gross, Shixiang Shane Gu, Yufei Guo, Chris Hallacy, Jesse Han, Jeff Harris, Yuchen He, Mike Heaton, Johannes Heidecke, Chris Hesse, Alan Hickey, Wade Hickey, Peter Hoeschele, Brandon Houghton, Kenny Hsu, Shengli Hu, Xin Hu, Joost Huizinga, Shantanu Jain, Shawn Jain, Joanne Jang, Angela Jiang, Roger Jiang, Haozhun Jin, Denny Jin, Shino Jomoto, Billie Jonn, Heewoo Jun, Tomer Kaftan, Łukasz Kaiser, Ali Kamali, Ingmar Kanitscheider, Nitish Shirish Keskar, Tabarak Khan, Logan Kilpatrick, Jong Wook Kim, Christina Kim, Yongjik Kim, Jan Hendrik Kirchner, Jamie Kiros, Matt Knight, Daniel Kokotajlo, Łukasz Kondraciuk, Andrew Kondrich, Aris Konstantinidis, Kyle Kopic, Gretchen Krueger, Vishal Kuo, Michael Lampe, Ikai Lan, Teddy Lee, Jan Leike, Jade Leung, Daniel Levy, Chak Ming Li, Rachel Lim, Molly Lin, Stephanie Lin, Mateusz Litwin, Theresa Lopez, Ryan Lowe, Patricia Lue, Anna Makanju, Kim Malfacini, Sam Manning, Todor Markov, Yaniv Markovski, Bianca Martin, Katie Mayer, Andrew Mayne, Bob McGrew, Scott Mayer McKinney, Christine McLeavey, Paul McMillan, Jake McNeil, David Medina, Aalok Mehta, Jacob Menick, Luke Metz, Andrey Mishchenko, Pamela Mishkin, Vinnie Monaco, Evan Morikawa, Daniel Mossing, Tong Mu, Mira Murati, Oleg Murk, David Mély, Ashvin Nair, Reiichiro Nakano, Rameev Nayak, Arvind Neelakantan, Richard Ngo, Hyeonwoo Noh, Long Ouyang, Cullen O’Keefe, Jakub Pachocki, Alex Paino, Joe Palermo, Ashley Pantuliano, Giambattista Parascandolo, Joel Parish, Emy Parparita, Alex Passos, Mikhail Pavlov, Andrew Peng, Adam Perelman, Filipe de Avila Belbute Peres, Michael Petrov, Henrique Ponde de Oliveira Pinto, Michael, Pokorny, Michelle Pokrass, Vitchyr H. Pong, Tolly Powell, Alethea Power, Boris Power, Elizabeth Proehl, Raul Puri, Alec Radford, Jack Rae, Aditya Ramesh, Cameron Raymond, Francis Real, Kendra Rimbach, Carl Ross, Bob Rotsted, Henri Roussez, Nick Ryder, Mario Saltarelli, Ted Sanders, Shibani Santurkar, Girish Sastry, Heather Schmidt, David Schnurr, John Schulman, Daniel Selsam, Kyla Sheppard, Toki Sherbakov, Jessica Shieh, Sarah Shoker, Pranav Shyam, Szymon Sidor, Eric Sigler, Maddie Simens, Jordan Sitkin, Katarina Slama, Ian Sohl, Benjamin Sokolowsky, Yang Song, Natalie Staudacher, Felipe Petroski Such, Natalie Summers, Ilya Sutskever, Jie Tang, Nikolas Tezak, Madeleine B. Thompson, Phil Tillet, Amin Tootoonchian, Elizabeth Tseng, Preston Tuggle, Nick Turley, Jerry Tworek, Juan Felipe Cerón Uribe, Andrea Vallone, Arun Vijayvergiya, Chelsea Voss, Carroll Wainwright, Justin Jay Wang, Alvin Wang, Ben Wang, Jonathan Ward, Jason Wei, CJ Weinmann, Akila Welihinda, Peter Welinder, Jiayi Weng, Lilian Weng, Matt Wiethoff, Dave Willner, Clemens Winter, Samuel Wolrich, Hannah Wong, Lauren Workman, Sherwin Wu, Jeff Wu, Michael Wu, Kai Xiao, Tao Xu, Sarah Yoo, Kevin Yu, Qiming Yuan, Wojciech Zaremba, Rowan Zellers, Chong Zhang, Marvin Zhang, Shengjia Zhao, Tianhao Zheng, Juntang Zhuang, William Zhuk, and Barret Zoph. Gpt-4 technical report. *arXiv preprint arXiv:2303.08774*, 2024.

- [40] Songyou Peng, Kyle Genova, Chiyu Jiang, Andrea Tagliasacchi, Marc Pollefeys, Thomas Funkhouser, et al. Openscene: 3d scene understanding with open vocabularies. In *Proceedings of the IEEE/CVF Conference on Computer Vision and Pattern Recognition*, pages 815–824, 2023.
- [41] Ben Poole, Ajay Jain, Jonathan T Barron, and Ben Mildenhall. Dreamfusion: Text-to-3d using 2d diffusion. *arXiv preprint arXiv:2209.14988*, 2022.
- [42] Alec Radford, Jong Wook Kim, Chris Hallacy, Aditya Ramesh, Gabriel Goh, Sandhini Agarwal, Girish Sastry, Amanda Askell, Pamela Mishkin, Jack Clark, et al. Learning transferable visual models from natural language supervision. In *International conference on machine learning*, pages 8748–8763. PMLR, 2021.
- [43] Alec Radford, Jeffrey Wu, Rewon Child, David Luan, Dario Amodei, Ilya Sutskever, et al. Language models are unsupervised multitask learners. *OpenAI blog*, 1(8):9, 2019.
- [44] Aditya Sanghi, Hang Chu, Joseph G Lambourne, Ye Wang, Chin-Yi Cheng, Marco Fumero, and Kamal Rahimi Malekshan. Clip-forge: Towards zero-shot text-to-shape generation. In *Proceedings of the IEEE/CVF Conference on Computer Vision and Pattern Recognition*, pages 18603–18613, 2022.
- [45] David Stutz and Andreas Geiger. Learning 3d shape completion from laser scan data with weak supervision. In *Proceedings of the IEEE conference on computer vision and pattern recognition*, pages 1955–1964, 2018.
- [46] David Stutz and Andreas Geiger. Learning 3d shape completion under weak supervision. *International Journal of Computer Vision*, 128:1162–1181, 2020.
- [47] Lyne P Tchaptmi, Vineet Kosaraju, Hamid Rezafofighi, Ian Reid, and Silvio Savarese. Topnet: Structural point cloud decoder. In *Proceedings of the IEEE/CVF conference on computer vision and pattern recognition*, pages 383–392, 2019.
- [48] Gemma Team, Thomas Mesnard, Cassidy Hardin, Robert Dadashi, Surya Bhupatiraju, Shreya Pathak, Laurent Sifre, Morgane Rivière, Mihir Sanjay Kale, Juliette Love, et al. Gemma: Open models based on gemini research and technology. *arXiv preprint arXiv:2403.08295*, 2024.
- [49] Hugo Touvron, Thibaut Lavril, Gautier Izacard, Xavier Martinet, Marie-Anne Lachaux, Timothée Lacroix, Baptiste Rozière, Naman Goyal, Eric Hambro, Faisal Azhar, Aurelien Rodriguez, Armand Joulin, Edouard Grave, and Guillaume Lample. Llama: Open and efficient foundation language models. *arXiv preprint arXiv:2302.13971*, 2023.
- [50] Arash Vahdat, Francis Williams, Zan Gojcic, Or Litany, Sanja Fidler, Karsten Kreis, et al. Lion: Latent point diffusion models for 3d shape generation. *Advances in Neural Information Processing Systems*, 35:10021–10039, 2022.
- [51] Aaron van den Oord, Oriol Vinyals, and Koray Kavukcuoglu. Neural discrete representation learning. *arXiv preprint arXiv:1711.00937*, 2018.
- [52] Haochen Wang, Xiaodan Du, Jiahao Li, Raymond A Yeh, and Greg Shakhnarovich. Score jacobian chaining: Lifting pretrained 2d diffusion models for 3d generation. In *Proceedings of the IEEE/CVF Conference on Computer Vision and Pattern Recognition*, pages 12619–12629, 2023.
- [53] Wenhai Wang, Zhe Chen, Xiaokang Chen, Jiannan Wu, Xizhou Zhu, Gang Zeng, Ping Luo, Tong Lu, Jie Zhou, Yu Qiao, and Jifeng Dai. Visionllm: Large language model is also an open-ended decoder for vision-centric tasks. *arXiv preprint arXiv:2305.11175*, 2023.
- [54] Zehan Wang, Haifeng Huang, Yang Zhao, Ziang Zhang, and Zhou Zhao. Chat-3d: Data-efficiently tuning large language model for universal dialogue of 3d scenes. *arXiv preprint arXiv:2308.08769*, 2023.
- [55] Zhengyi Wang, Cheng Lu, Yikai Wang, Fan Bao, Chongxuan Li, Hang Su, and Jun Zhu. Prolificdreamer: High-fidelity and diverse text-to-3d generation with variational score distillation. *Advances in Neural Information Processing Systems*, 36, 2024.
- [56] Xin Wen, Peng Xiang, Zhizhong Han, Yan-Pei Cao, Pengfei Wan, Wen Zheng, and Yu-Shen Liu. Pmp-net: Point cloud completion by learning multi-step point moving paths. In *Proceedings of the IEEE/CVF conference on computer vision and pattern recognition*, pages 7443–7452, 2021.
- [57] Jiajun Wu, Chengkai Zhang, Xiuming Zhang, Zhoutong Zhang, William T. Freeman, and Joshua B. Tenenbaum. Learning shape priors for single-view 3d completion and reconstruction. In *Proceedings of the European Conference on Computer Vision (ECCV)*, September 2018.
- [58] Rundi Wu, Xuelin Chen, Yixin Zhuang, and Baoquan Chen. Multimodal shape completion via conditional generative adversarial networks. In *Computer Vision—ECCV 2020: 16th European Conference, Glasgow, UK, August 23–28, 2020, Proceedings, Part IV 16*, pages 281–296. Springer, 2020.
- [59] Zhennan Wu, Yang Li, Han Yan, Taizhang Shang, Weixuan Sun, Senbo Wang, Ruikai Cui, Weizhe Liu, Hiroyuki Sato, Hongdong Li, et al. Blockfusion: Expandable 3d scene generation using latent tri-plane extrapolation. *arXiv preprint arXiv:2401.17053*, 2024.

- [60] Zhirong Wu, Shuran Song, Aditya Khosla, Fisher Yu, Linguang Zhang, Xiaoou Tang, and Jianxiong Xiao. 3d shapenets: A deep representation for volumetric shapes. In *Proceedings of the IEEE conference on computer vision and pattern recognition*, pages 1912–1920, 2015.
- [61] Xingguang Yan, Liqiang Lin, Niloy J Mitra, Dani Lischinski, Daniel Cohen-Or, and Hui Huang. Shapeformer: Transformer-based shape completion via sparse representation. In *Proceedings of the IEEE/CVF Conference on Computer Vision and Pattern Recognition*, pages 6239–6249, 2022.
- [62] Jianing Yang, Xuweiyi Chen, Shengyi Qian, Nikhil Madaan, Madhavan Iyengar, David F Fouhey, and Joyce Chai. Llm-grounder: Open-vocabulary 3d visual grounding with large language model as an agent. *arXiv preprint arXiv:2309.12311*, 2023.
- [63] Fukun Yin, Xin Chen, Chi Zhang, Biao Jiang, Zibo Zhao, Jiayuan Fan, Gang Yu, Taihao Li, and Tao Chen. Shapegpt: 3d shape generation with a unified multi-modal language model. *arXiv preprint arXiv:2311.17618*, 2023.
- [64] Xumin Yu, Yongming Rao, Ziyi Wang, Zuyan Liu, Jiwen Lu, and Jie Zhou. Pointr: Diverse point cloud completion with geometry-aware transformers. In *ICCV*, 2021.
- [65] Xumin Yu, Lulu Tang, Yongming Rao, Tiejun Huang, Jie Zhou, and Jiwen Lu. Point-bert: Pre-training 3d point cloud transformers with masked point modeling. In *Proceedings of the IEEE/CVF conference on computer vision and pattern recognition*, pages 19313–19322, 2022.
- [66] Wentao Yuan, Tejas Khot, David Held, Christoph Mertz, and Martial Hebert. Pcn: Point completion network. In *2018 international conference on 3D vision (3DV)*, pages 728–737. IEEE, 2018.
- [67] Hang Zhang, Xin Li, and Lidong Bing. Video-llama: An instruction-tuned audio-visual language model for video understanding. *arXiv preprint arXiv:2306.02858*, 2023.
- [68] Junzhe Zhang, Xinyi Chen, Zhongang Cai, Liang Pan, Haiyu Zhao, Shuai Yi, Chai Kiat Yeo, Bo Dai, and Chen Change Loy. Unsupervised 3d shape completion through gan inversion. In *Proceedings of the IEEE/CVF Conference on Computer Vision and Pattern Recognition (CVPR)*, pages 1768–1777, June 2021.
- [69] Linqi Zhou, Yilun Du, and Jiajun Wu. 3d shape generation and completion through point-voxel diffusion. In *Proceedings of the IEEE/CVF international conference on computer vision*, pages 5826–5835, 2021.

## A Implementation Details

**Dataset preparation** We randomly selected 3130 data from ShapeNetCore [6], and randomly split data of each category into 90% training data and 10% testing data.

**Model structure** We present the hyperparameters in Tab. 6. Those values can determine the detailed structures of each component in our pipeline.

<b>HYPERPARAMETER</b>	<b>VALUE</b>
VAE Encoder Convolution Layer Num	2
VAE Decoder Convolution Layer Num	2
VAE Hidden Dimension	64
VAE Latent Size	128
LoRA Rank	32
LoRA Alpha	32
LoRA Dropout	0.05
LLM Type	Mistral-7B
Output Projection Transformer Encoder Layer Num	2
Output Projection Transformer Decoder Layer Num	2
Output Projection Transformer Feedforward Dimension	2048
Output Projection Transformer Num Heads	4

Table 6: Hyperparameters used to configure model structure.

**Training configuration** We train our patch VAE on 2 RTX 4090 cards for 100 epochs and batch size using ShapeNet voxels volumes with resolution  $64^3$  and adopt the same VAE for voxels with different resolutions. This training takes approximately 2 hours. The model is trained with AdamW [35] optimizer with a learning rate  $3e^{-4}$ .

Our input projection and output projection models are trained on 8 RTX 6000 Ada GPU cards until converge, for around 100 and 500 epochs respectively. For Mistral-7B, these processes take around 1 hour and 18 hours, respectively, while for Gemma-2B, the numbers go down to 20 minutes and 8 hours. Both stages are trained with AdamW optimizer as well, with input projection training using a learning rate of  $3e^{-4}$  and output projection training using  $5e^{-4}$  or  $5e^{-5}$ , depending on the LLM size.

## B Examples of Ground-Truth and Predicted Captions

Here we present some examples of ground-truth captions and the captions predicted by our LLM model during input projection layer training. We notice that the captions are not perfect, while they provide adequate semantic meanings.

PREDICTED CAPTION 1: 3AD model of a ", featuring a exterior such as wings, fuselage, and, andinglets, and, and, andilerons, and flaps" with for 3 and7-400 and 747-800 variants.",

GROUND-TRUTH CAPTION 1: "3D model of Boeing aircraft, featuring detailed components such as wings, fuselage, tail, winglets, rudder, elevators, ailerons, and flaps, available in both 747-400 and 737-800 variants."

PREDICTED CAPTION 2: 3D model of a rectangular 737- featuring a fuselage body with a wings, and tail tail tail, and, and, andilerons, and a gear.,

GROUND-TRUTH CAPTION 2: 3D model of a Boeing 747, featuring a cylindrical fuselage, elliptical wings, a truncated cone tail, rudder, elevators, ailerons, and landing gear.

PREDICTED CAPTION 3: 3D model of of a guitars Ghostcar aircraft jets, including a-A-18E F-14., with for download3ds Max. OBJ.,

GROUND-TRUTH CAPTION 3: 3D model collection of various Phantom and Super Hornet fighter jets, including F/A-18 and F-16 variants, available for 3ds Max and Maya.

PREDICTED CAPTION 4: 3D model of a rectangular 737-800 aircraft a fuselage dome, with a conelate spher, and a- a. steel.,

GROUND-TRUTH CAPTION 4: 3D model of a Boeing 747-400 featuring a spherical fuselage shell, truncated oblate wings, and made of aluminum and steel.

PREDICTED CAPTION 5: 3 with a cylindrical, a, and, and, and,, and landing landing gear.,

GROUND-TRUTH CAPTION 5: A spaceship featuring a wing, fuselage, tail, propeller, rotor blade, and retractable landing gear.

PREDICTED CAPTION 6: 3D model of a electric with a, a, and, and, and, andilerons, and gear, and a.,

GROUND-TRUTH CAPTION 6: 3D model of an aircraft featuring wings, fuselage, tail, rudder, elevators, ailerons, landing gear, and propeller.

PREDICTED CAPTION 7: 3Aalty-free 3D model of a female 737-400 aircraft featuring a exterior such as a fuselage, fuselage, and tail.",

GROUND-TRUTH CAPTION 7: "Royalty-free 3D model of a Boeing 747-400, featuring detailed components such as a wing, fuselage, and tail."

PREDICTED CAPTION 8: 3D model of a rectangularliner with a fuselage wing, a fuselage, and, and, andders, and, and gear, and landing.,

GROUND-TRUTH CAPTION 8: 3D model of a jet plane featuring a delta wing, triangular fuselage, tail, fin, rudders, propeller, landing gear, and hull.

## C Illustrations of Data Augmentation

**3D Data Augmentation** During training, we performed 3D augmentation by randomly rotating each 3D object with a different angle with respect to either  $x$ ,  $y$ , or  $z$  axis. Figure 4 visualizes this result.

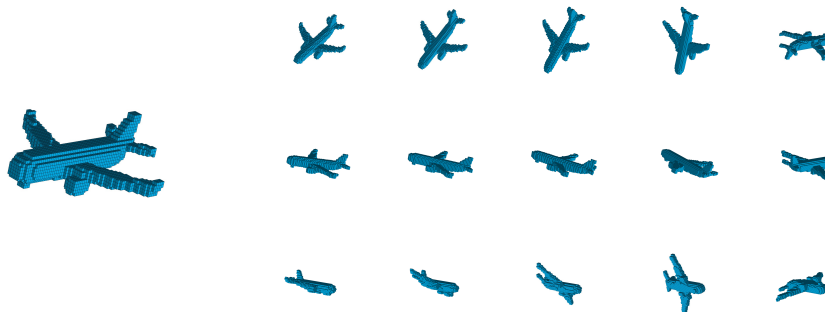


Figure 4: 3D data augmentation example result of an airplane.

**Caption Augmentation** During training, we leveraged Cap3D [37] to generate ground-truth captions for every 3D model. To perform caption augmentation, we run Cap3D for three times, using GPT-4-Turbo, GPT-4-Turbo with another seed, and ChatGPT (GPT-3.5). Here we present the captions generated by them.



Figure 5: From left to right: Object 1, 2, 3, 4.

Captions for Object 1:

GPT-4 SEED 1: Royalty-free 3D model of a Boeing 747-400 featuring detailed components including a cylindrical fuselage, delta wings, tail, rudder, elevators, and ailerons.

GPT-4 SEED 2: Royalty-free 3D model of a Boeing 747-400 featuring a cylindrical fuselage, delta wings, a tail, rudder, elevators, and ailerons, representing a four-engine jet airliner.

CHATGPT: Boeing 747-400 3D model featuring a fuselage, wings, and tail, a jumbo jet with a delta wing design and four engines.

Captions for Object 2:

GPT-4 SEED 1: A 3D model of a two-seater, single-engine RC airplane featuring a four-bladed, fixed-pitch propeller, retractable tricycle landing gear, and control surfaces including ailerons, rudder, and elevator.

GPT-4 SEED 2: A 3D model of a small, two-seater, single-engine RC airplane featuring a retractable tricycle landing gear, a fixed-pitch, four-bladed propeller, and control surfaces including wings, fuselage, tail, rudder, elevator, and ailerons.

CHATGPT: 3D model of a two-seater single-engine airplane with retractable landing gear and a four-bladed propeller.

Captions for Object 3:

GPT-4 SEED 1: Royalty-free 3D model of a blue McLaren MP4-12C sports car with polygonal geometry.

GPT-4 SEED 2: Royalty-free 3D model of a McLaren MP4-12C sports car with polygonal geometry.

CHATGPT: 3D model of a McLaren MP4-12C sports car.

Captions for Object 4:

GPT-4 SEED 1: 3D model of a police car, available royalty-free, featuring detailed polygonal geometry.

GPT-4 SEED 2: 3D model of a police car, featuring detailed polygonal vertices and edges, available royalty-free.

CHATGPT: A detailed 3D model of a police car.

## D Unlock Better Quality via Iterative Completion

We also found that our model is able to refine the results without further training, by directly passing the output from the last step and the caption into our model. We show this using the denoising example as the changes are more obvious. After applying the denoising twice, we observe that the quality in Fig. 6 has significantly increased.

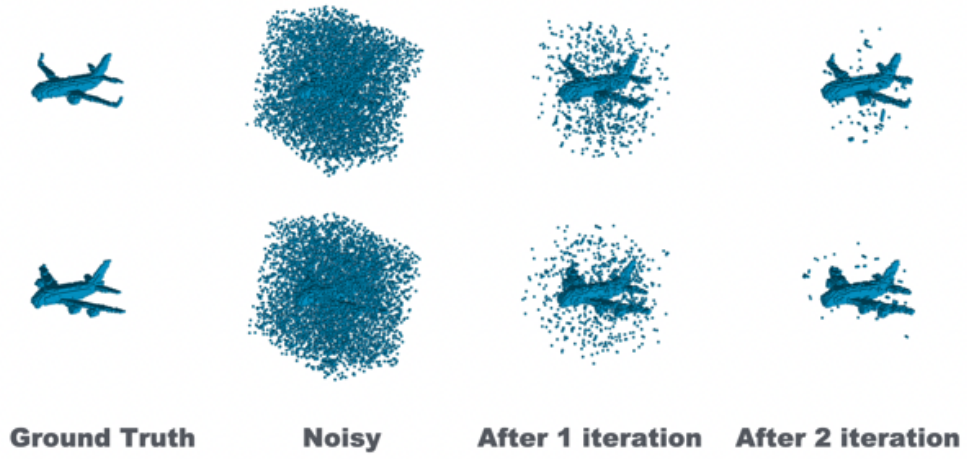


Figure 6: Result on Iterative Denoising

## E More Results

Figure 7 to 16 present more results of more categories, notice that all these results are inferred from the same checkpoint as used in the experiment session.

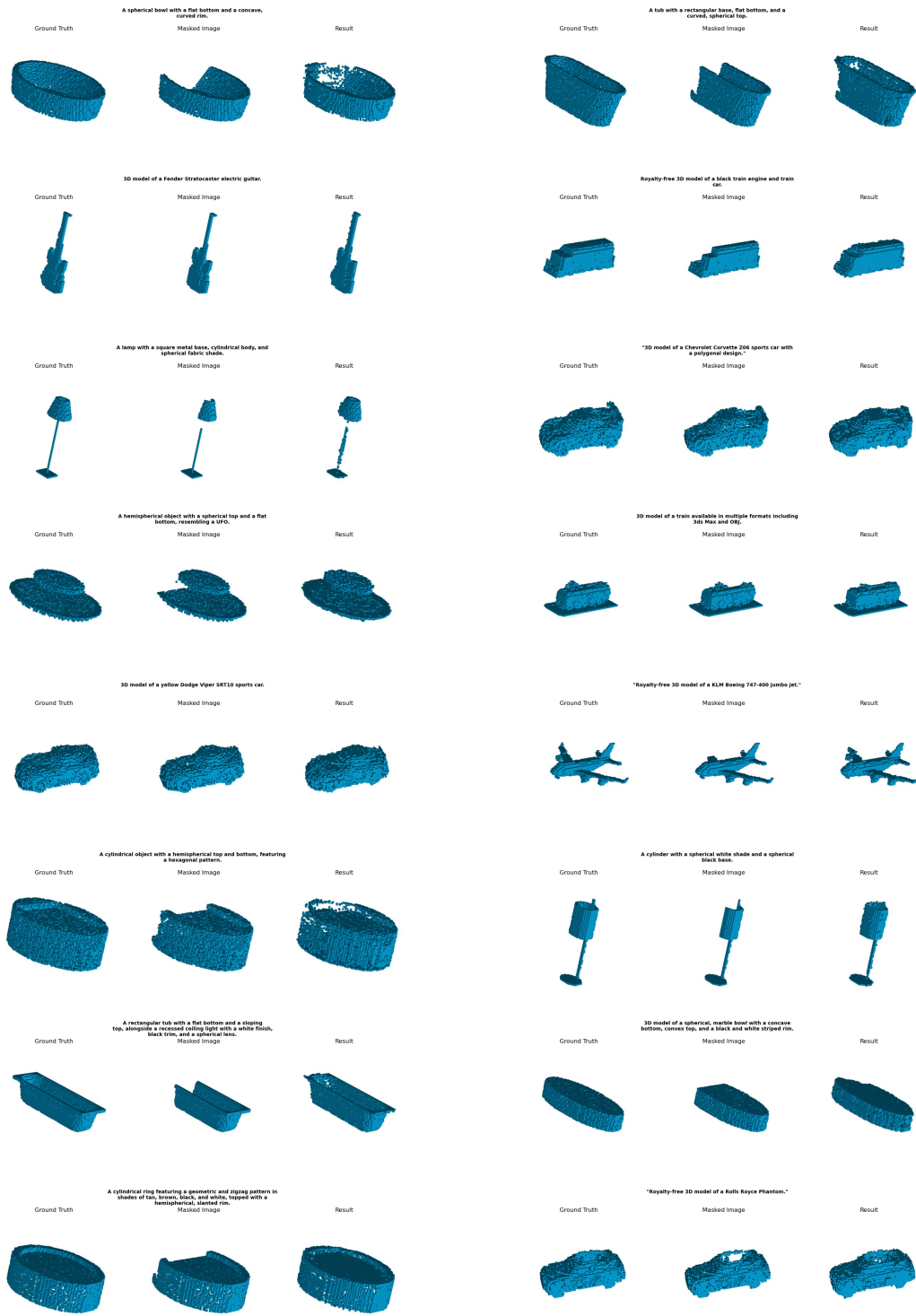


Figure 7: Results Seg20%

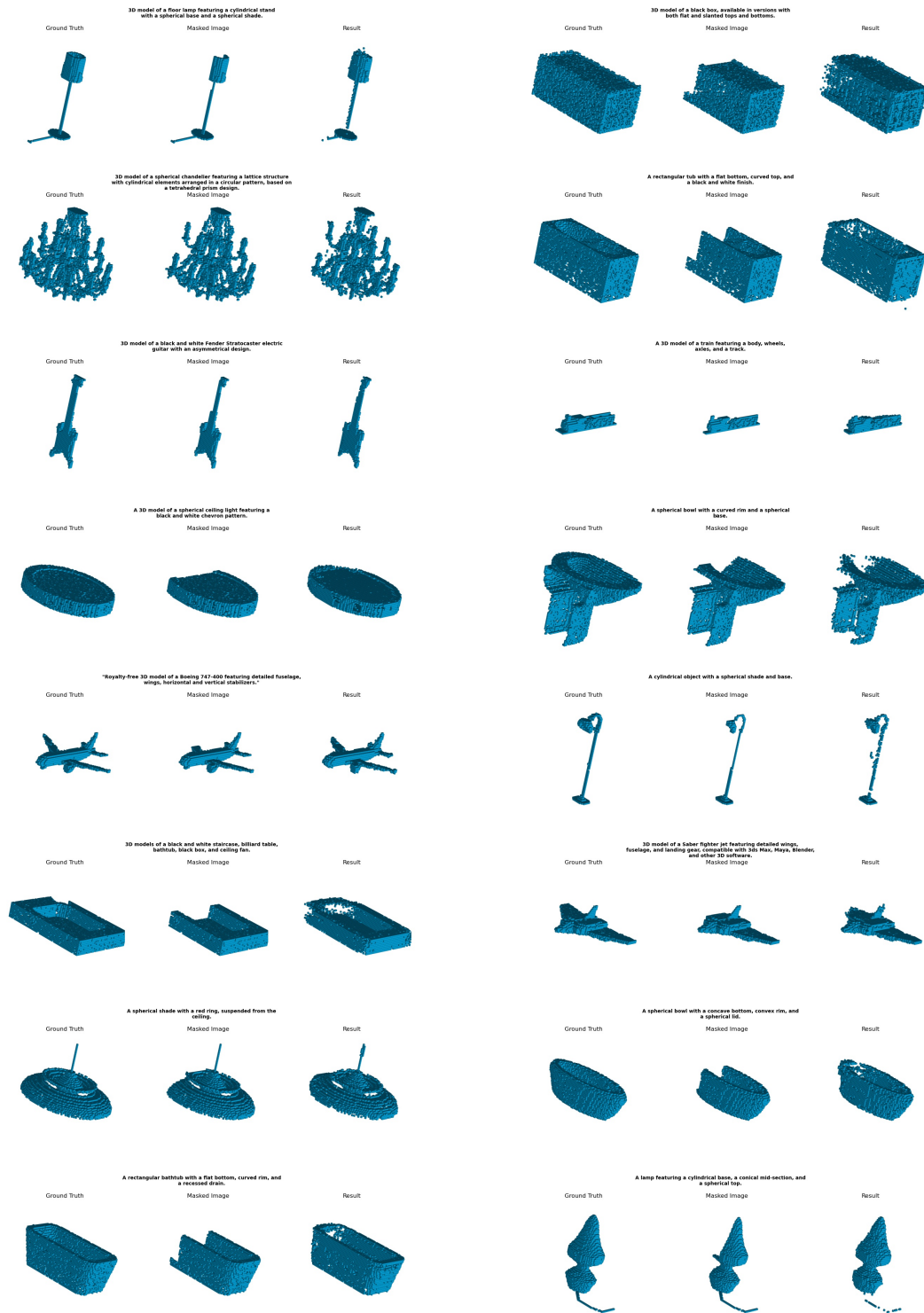


Figure 8: Results Seg20%

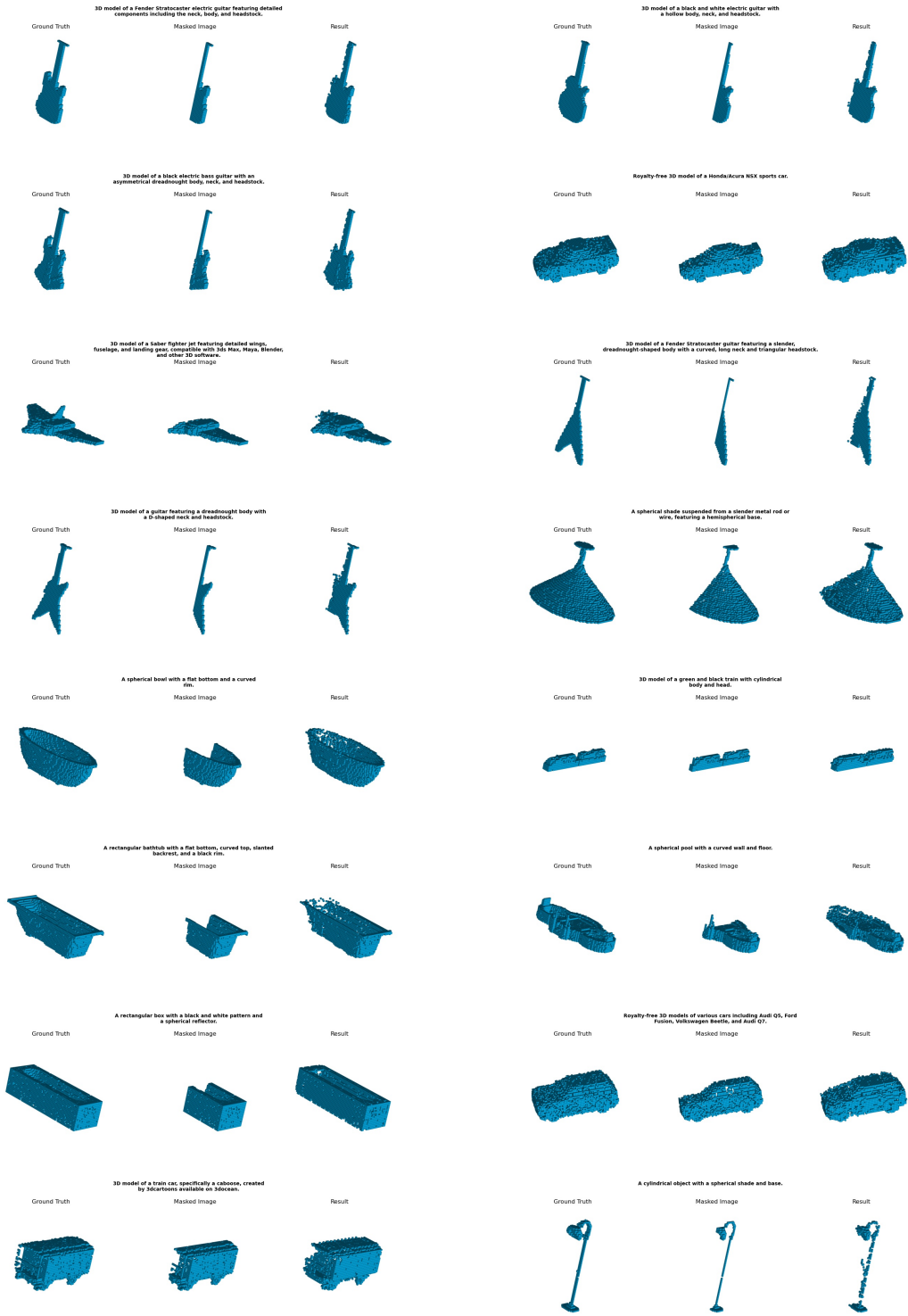


Figure 9: Results Seg50%

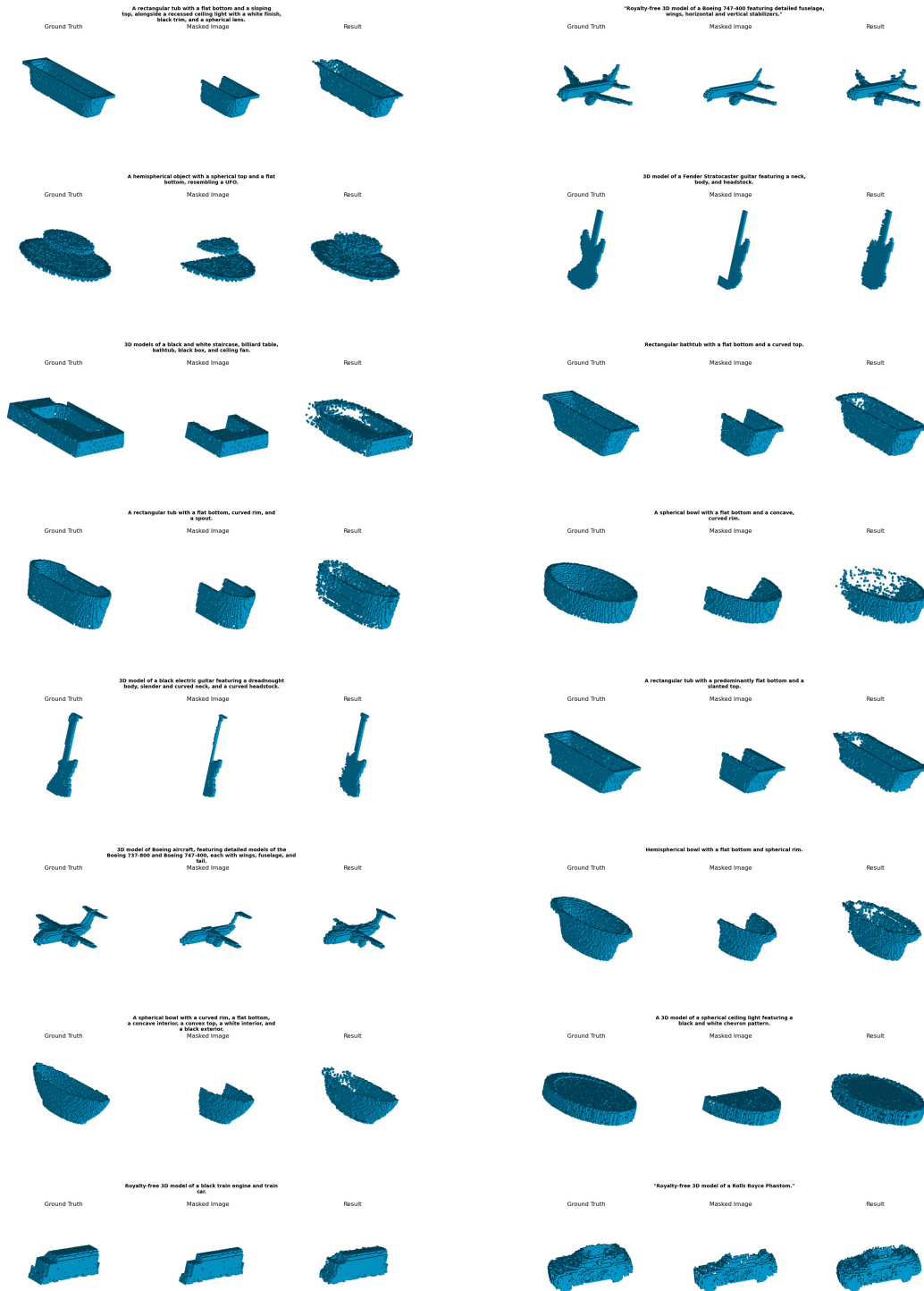


Figure 10: Results Seg50%

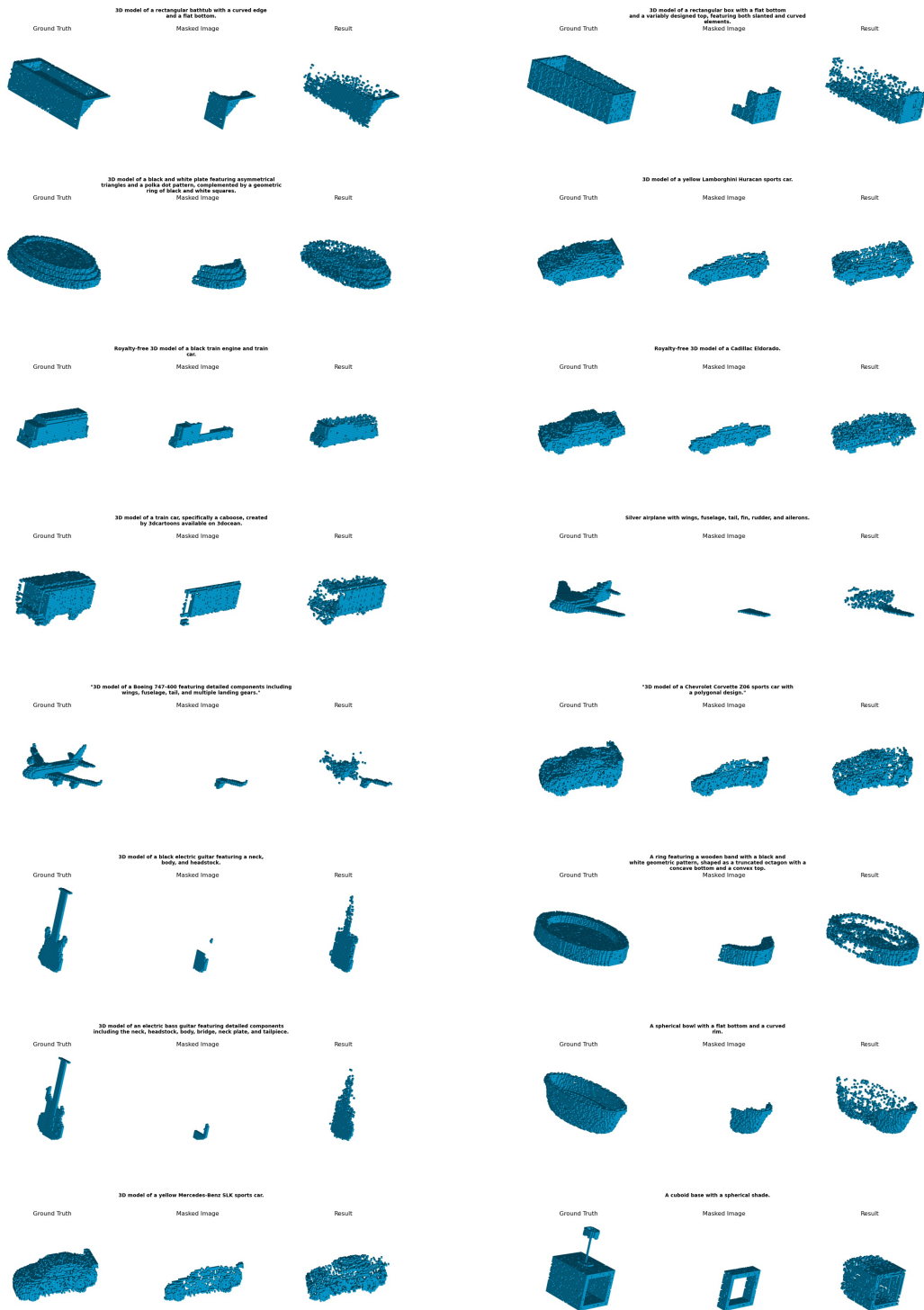


Figure 11: Results Seg80%

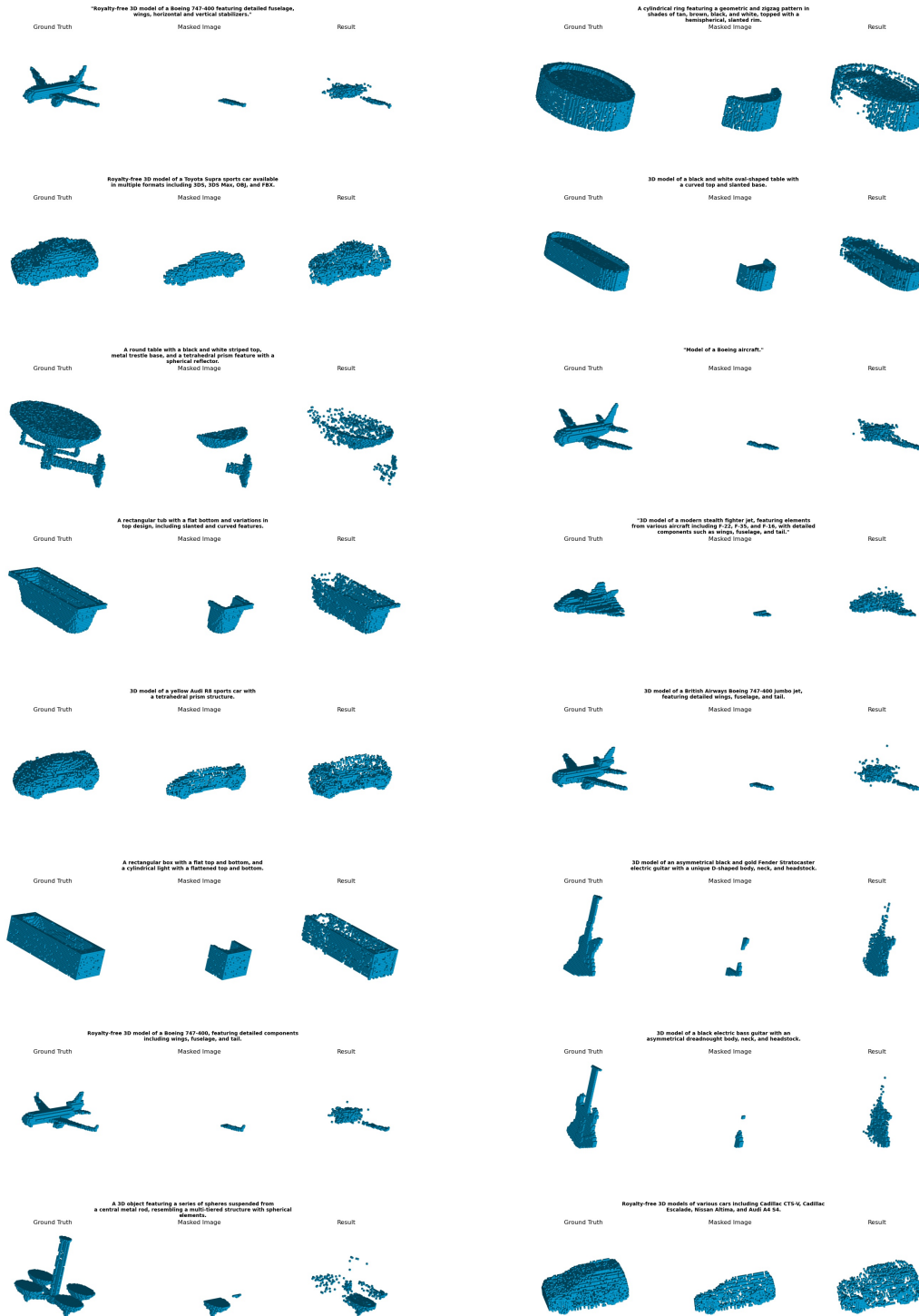


Figure 12: Results Seg80%

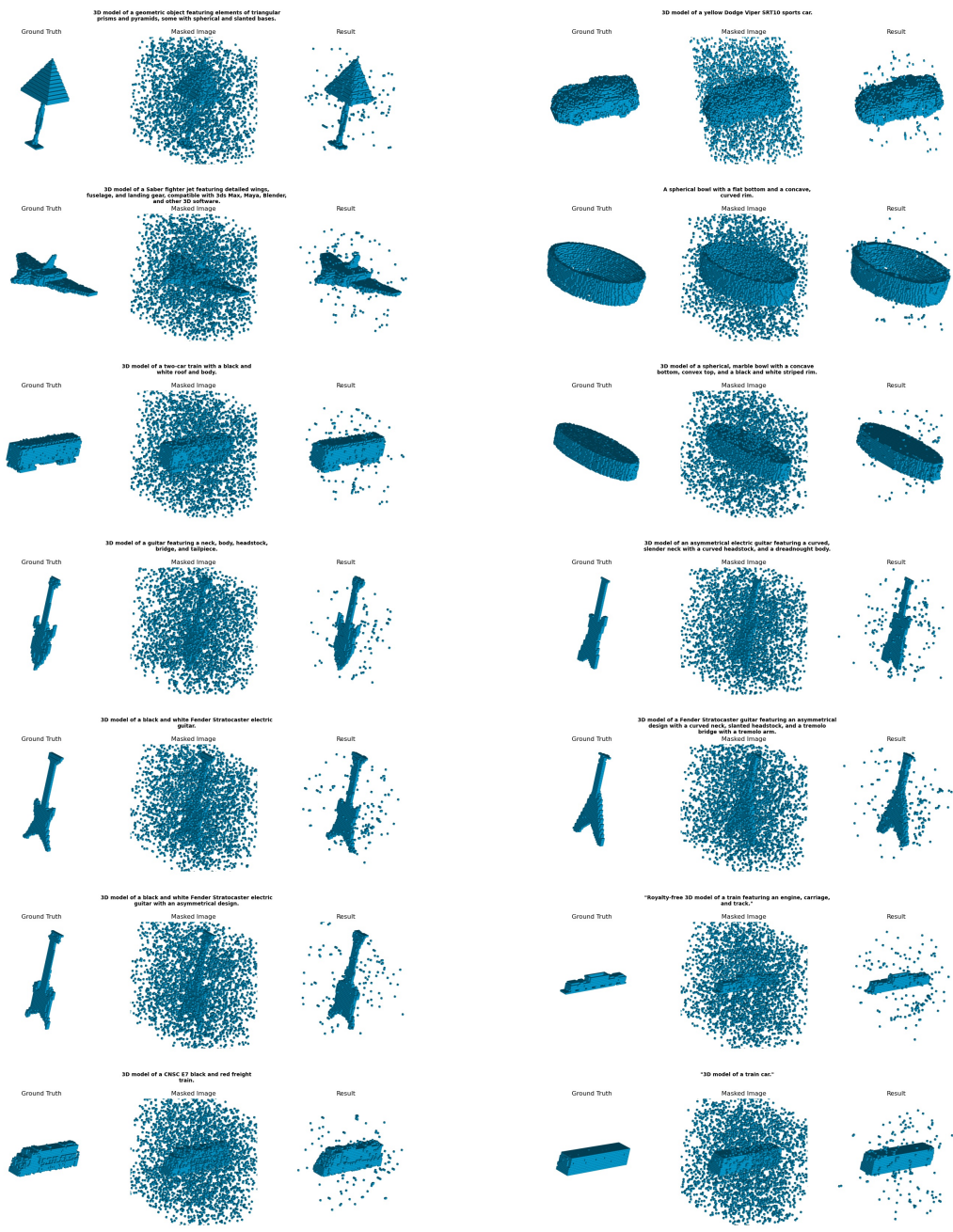


Figure 13: Results Noise1%

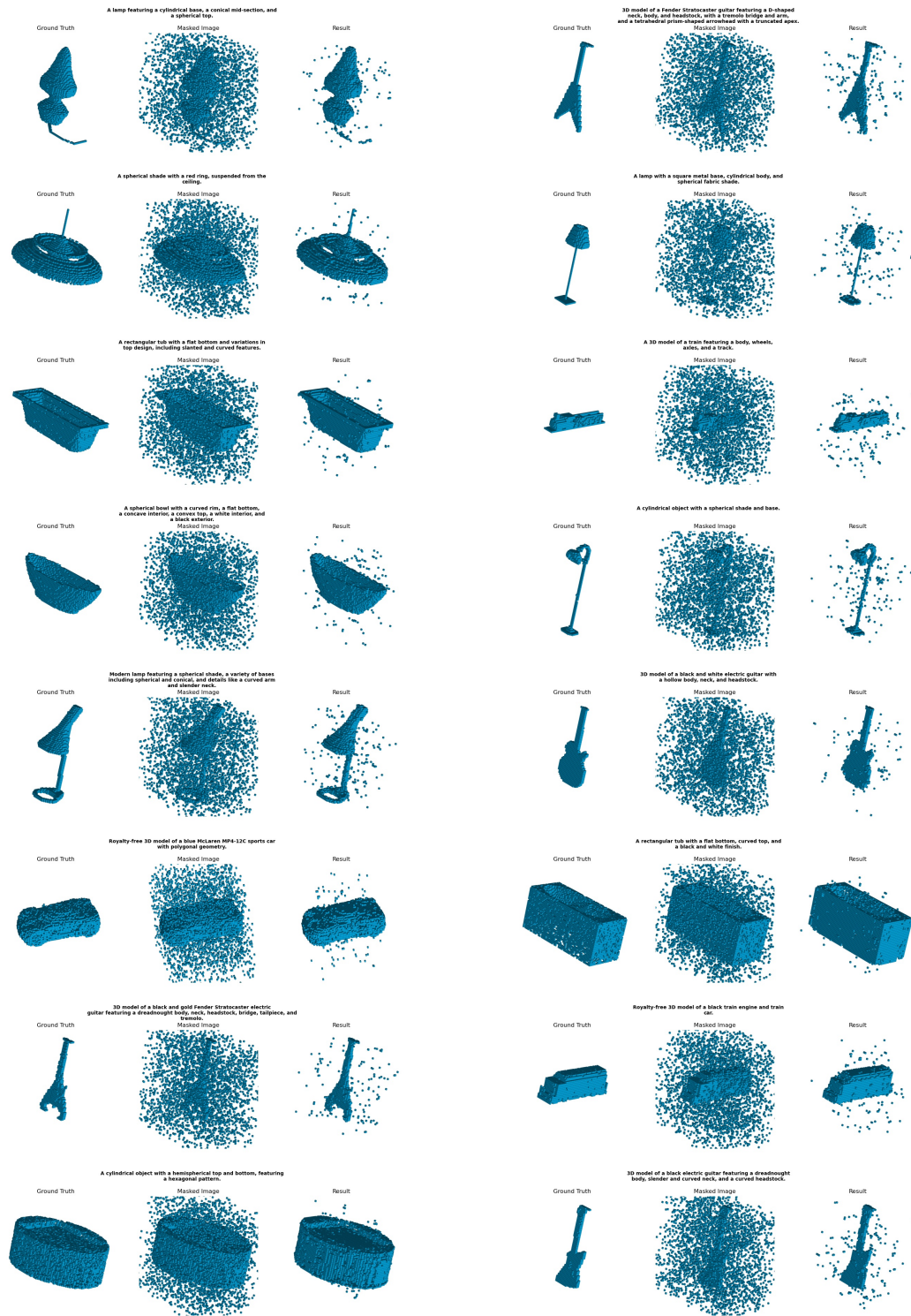


Figure 14: Results Noise1%

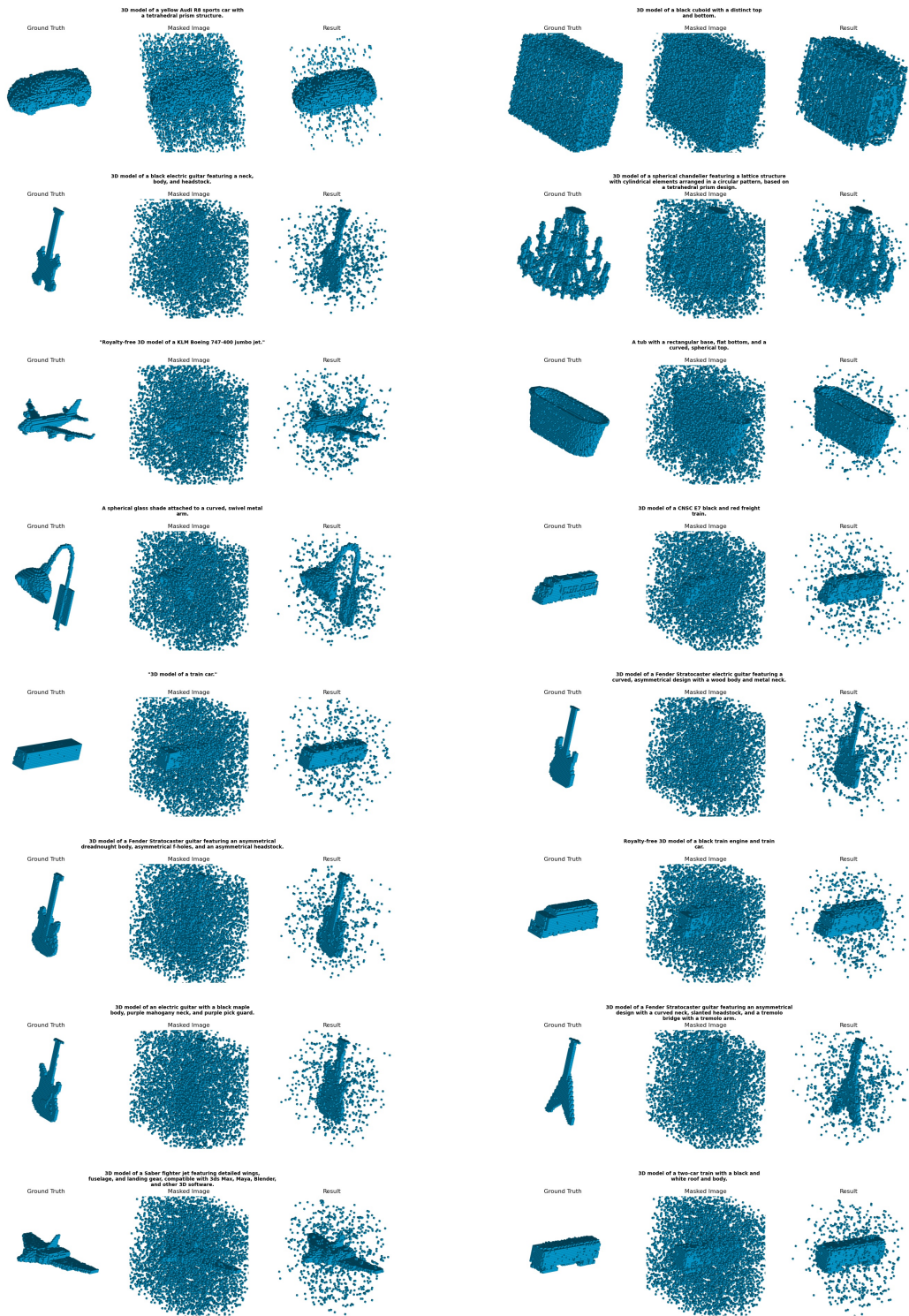


Figure 15: Results Noise2%

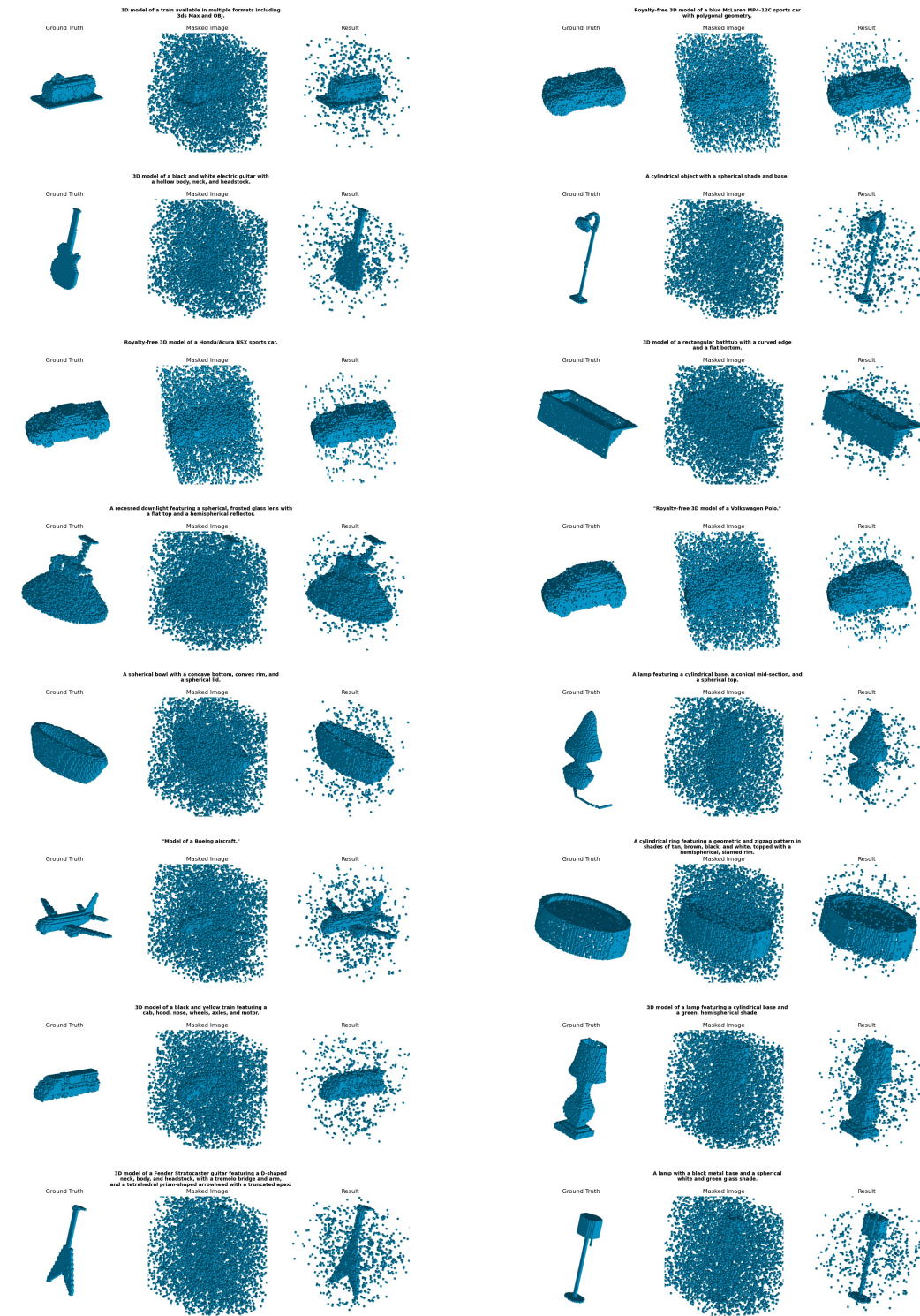


Figure 16: Results Noise2%